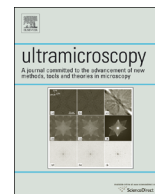




ELSEVIER

Contents lists available at ScienceDirect

Ultramicroscopy

journal homepage: www.elsevier.com/locate/ultramic

On the interaction of an ultra-fast laser with a nanometric tip by laser assisted atom probe tomography: A review



A. Vella*

Groupe de Physique des Materiaux UMR CNRS 6634, UFR Sciences Site du Madrillet, Avenue de l'Université - B.P. 12 76801 Saint Etienne du Rouvray Cedex, France

ARTICLE INFO

Available online 11 June 2013

Keywords:

Optical nano-object
Field emission
Atom probe

ABSTRACT

The evaporation mechanisms of surface atoms in laser assisted atom probe tomography (LA-APT) are reviewed with an emphasis on the changes in laser-matter interaction when the sample is a nanometric tip submitted to a high electric field. The nanometric dimensions induce light diffraction, the tip shape induces field enhancement and these effects together completely change the absorption properties of the sample from those of macroscopic bulk materials. Moreover, the high electric field applied to the sample during LA-APT analysis strongly modifies the surface optical properties of band gap materials, due to the band bending induced at the surface. All these effects are presented and studied in order to determine the physical mechanisms of atoms evaporation in LA-APT. Moreover, LA-APT is used as an original experimental setup to study: (a) the absorption of nanometric tips; (b) the contribution of the standing field to this laser energy absorption and (c) the heating and cooling process of nanometric sample after the interaction with ultra fast laser.

© 2013 Elsevier B.V. All rights reserved.

1. Introduction

In Atom Probe Tomography (APT) atoms are field evaporated from the surface of a tip-like shape specimen at a high positive voltage [1–3]. Surface atoms evaporated by sequence of high voltage pulsed field (HV) or laser pulses can be identified by time of flight mass spectroscopy. The composition of a small volume in the bulk can be analyzed at nearly atomic resolution. The atoms removed from the surface are radially projected onto a position-sensitive detector and, thanks to the projection law, they are positioned in each layer of the specimen (see Fig. 1(a)). Over the past several years this technique has been used to study various topics in material science [4,5]. The conventional APT uses nano-second high voltage pulses. Hence, this technique has only been applied to metallic samples due to the inability to transmit these pulses through sample tips of low electrical conductivity. Moreover, the longer duration of the HV pulses as compared to the vibration time of surface atoms results in a significant spread in the energy of emitted ions. This leads to a poor mass resolution in the straight APT if no energy compensating device is used.

Around the end of the 1970s was demonstrated that the use of laser pulses makes it possible to field evaporate surface atoms [6–8]. In the case of metals, as expected, the very short duration of the laser

pulse significantly reduces the ion energy distribution spread [9,4]. In the case of materials with low electrical conductivity, the use of the laser pulses allows the well controlled evaporation of surface atoms and opens the APT technique to nonconductive materials [10].

Hence, in laser assisted APT (LA-APT), atoms are ejected from a nanometric tip as a result of a joint action of an external high electric field of tens of V/nm and a laser pulse [4,11].

As LA-APT, many other techniques are based on the interaction between a laser beam and a nanometric tip under a high electric field such as photon-assisted scanning tunneling microscopy (p-STM) [12] or photon assisted electrons emission (p-EE) [13,14]. For all these applications, the laser-tip interaction causes linear and nonlinear optical effects (field enhancement, second harmonic generation, optical rectification, etc) [13,15] but it also induces heating of the tip. The evaluation of the absorption and heating of the tip becomes a key factor in the estimation of the contribution of thermal effect compared to optical effects on the underlying physical mechanism of each technique. For example, the surface structuring by p-STM can be due to the strong field enhancement at the tip apex or due to the thermal-induced mechanical contact [12,16]. Similarly, the electrons or ions ejection in p-EE or in LA-APT can be thermally or optically assisted [13,14,17,18]. Several models have been developed in all these different domains to evaluate the contribution of the thermal and optical effects, however the role of the standing electric field applied to the tip was generally neglected. In LA-APT and in p-STM, the standing electric field generated at the tip apex of several Volts/nm and this strong field can affect the optical properties

* Tel.: +33 232955168.

E-mail address: angela.vella@univ-rouen.fr

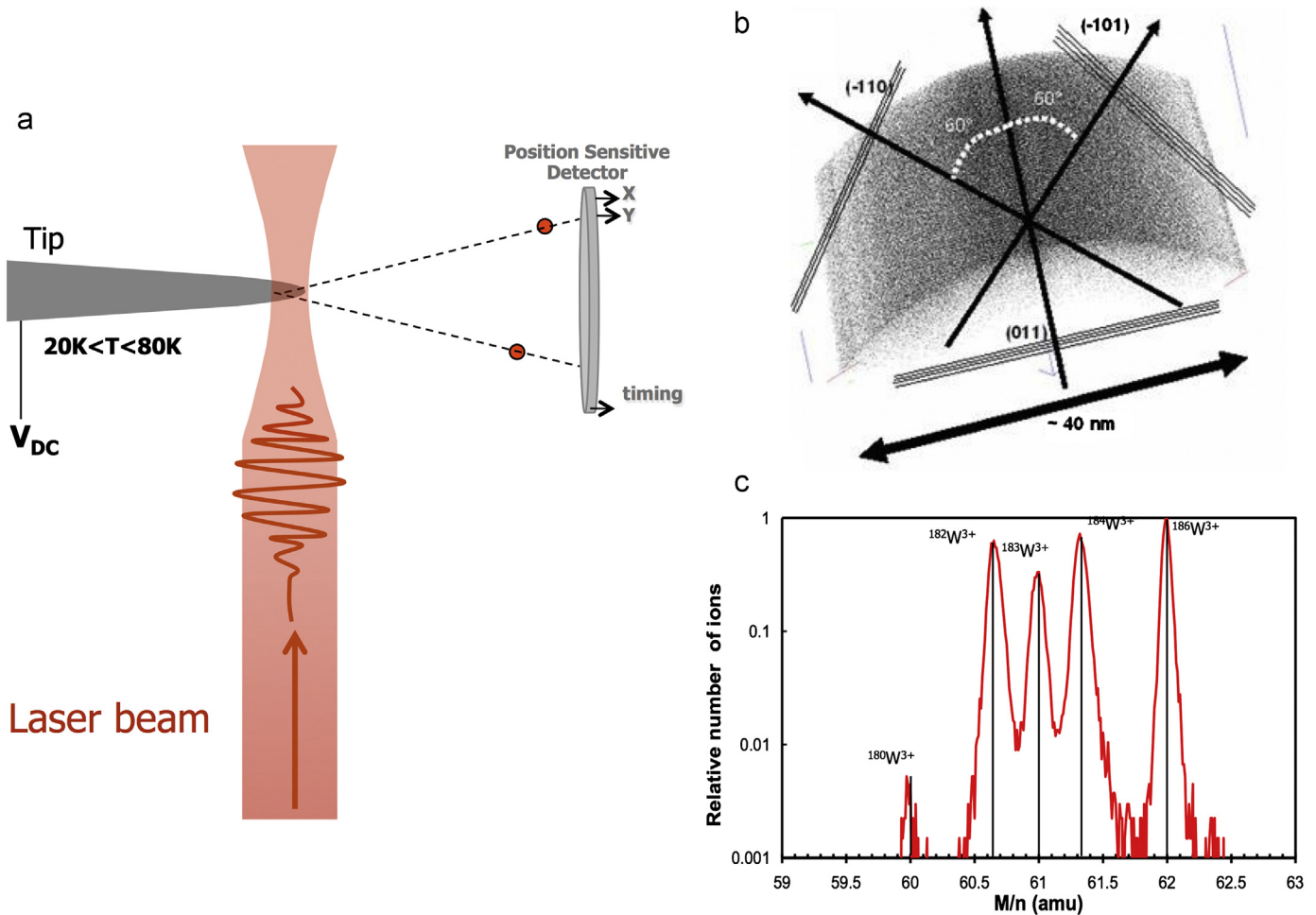


Fig. 1. (a) Schematic diagrams of the laser assisted atom probe, (b) surface image of evaporated ions reconstructed from the impact position on the detector, (c) mass spectrum of a tungsten tip.

of the tip, especially in the case of semiconductors, as theoretically studied by Tsong and Ernst in 1979 [19,20].

In this article the interaction between a nanometric tip and a laser beam is considered. Taking into account the effect of the high electric field applied to the tip, the main evaporation mechanisms of the surface atoms of metallic and nonmetallic tips in the LA-APT are determined.

2. Historical background of field evaporation assisted by laser pulses

When a positive electric field of several Volts/nm is applied on a metal surface, surface atoms evaporate in the form of ions. Two basic theories were developed to describe this phenomenon: the image force model [21] and the intersection model [4,22]. Both are based on a simple calculation of the field-evaporation activation energy Q_n , as the difference between the atomic and ionic potential energies for a metal atom on a metal surface. In the presence of an external field F_{DC} , the ionic states become more stable and the activation energy decreases with the applied field:

$$Q_n = \Lambda + \sum_n I_n - n\varphi_e - f(F_{DC}) \quad (1)$$

where Λ , I_n and φ_e are respectively the heat of sublimation, the n th ionization energy and the work function of the emitting surface, as reported in Fig. 2.

The expression of the function $f(F_{DC})$ depends on the model but, around the threshold of evaporation, a linear behavior of $f(F_{DC})$ was experimentally observed [23]. For a thermally activated field evaporation, the rate of process is given by the Arrhenius equation:

$$\phi = \nu \exp(-Q_n/k_B T) \quad (2)$$

where ν is the vibration frequency of the surface atoms, k_B the Boltzmann constant and T the emitter temperature. We can estimate the typical time τ_{evap} required for evaporating:

$$\tau_{evap} = \tau_0 \exp(Q_n/k_B T) \quad (3)$$

where τ_0 is the vibration time of surface atoms, typically a few picoseconds [24,25]. To chemically identify the evaporated atoms by time of flight mass spectrometry, a time-controlled field evaporation is ensured either by nanosecond high-voltage (HV) pulses superimposed to the standing voltage V_{DC} , or by laser pulses [4]. In the case of HV pulses, the duration of the pulses τ_p is typically of the order of 1 ns which is long enough to ensure field evaporation ($\tau_p > \tau_{evap}$).

When a laser pulse is used to trigger the evaporation, different evaporation mechanisms can occur:

1. the photo-ionization, corresponding to resonant ionization of surface atoms and its subsequent ejection as an ion;
2. the absorption of laser energy and the following heating of the specimen which allows thermal assisted evaporation;
3. the increase in the surface field which allows the evaporation by energy barrier reduction.

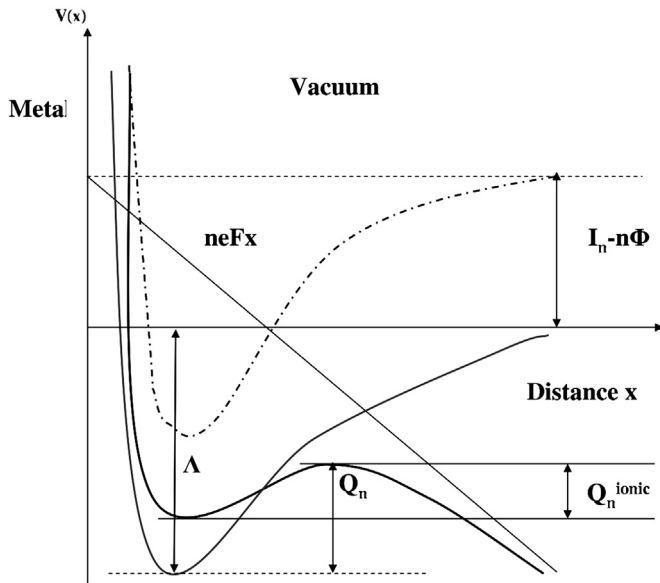


Fig. 2. Potential energy diagram of an atom under a standing electric field (thin line) and of an ion (thick line) at the surface of a metal. Dashed line: potential energy of atom without field.

Around the middle of the 1960s, the study of the interaction between a field emitter and a laser pulse started in the group of E. W. Muller. The laser they used was too powerful and unstable, hence the first experiments were unsuccessful. The first laser assisted AP analysis was reported around the end of the 1970s by Block and Tsong [6–8]. They replaced the high voltage pulses by nano or sub nano laser pulses in order to greatly improve the mass resolution by reducing the energy deficit and to enable the use of this instrument for non or poor conductive materials. New models for the laser-tip interaction were created while the first experiments on metal evaporation were taking place. At first, the purely quantum ionization process by resonant absorption of one or several photons was considered. The direct interaction between the photons and one atom can theoretically lead to its own ionization: one electron of the shell of the atom absorbs a photon and transmits it to the material. However, Viswanathan et al. [7] estimated that the lifetime of the holes in the energy levels of the metal or the atom are of about 10^{-15} s, which is much faster than the transition time through the potential barrier. This mechanism was thus quickly considered irrelevant in the case of metals, but it was reported in the case of a silicon tip by Tsong [9]. Indeed, in the case of semiconductors, due to the presence of a band gap, the lifetime of holes is longer than the evaporation time.

The thermal assisted evaporation, following the light's absorption by the sample and its resulting heating, was then considered. Kellogg and Tsong [26] and Kellogg [27] and Lee et Robins [28] showed experimentally that the temperature increase could be of a few hundred Kelvin, which corresponds to an energy of a few hundredth eV, sufficient to lead to a thermal assisted evaporation of the surface atoms.

Numerical and analytical models were developed to describe the tip's heating and cooling dynamics. For laser pulses of a few nanoseconds, taking into account the abnormal skin depth and the diffusivity length during the laser pulse, they concluded that sub-nanometric tips were heated uniformly only on one side of the cross section (as shown in Fig. 1(a)) [4]. For shorter laser pulses (100 ps), the diffraction effects, which predicted an homogeneous illumination of the tip's end, ensured homogeneous heating. They then considered that the heated zone size along the axis of the tip corresponded to

the zone illuminated by the laser, that is homogeneous heating in depth on a zone of several micrometers. Accounting for the cone shaped geometry of the tip, the calculated cooling time was of several nanoseconds for tungsten [29–31]. The same assumptions on the heated zone were made more recently by Ukraintsev et al. [12] to evaluate the heating of tungsten tips used in STM.

Slow cooling of the tip will lead to uncertainty in ion's evaporation time and thereby uncertainty in flight time resulting in poor mass resolution. Moreover, in these early experiments, it was very difficult to always focus the laser spot on the sample in the same way. Indeed, to ensure a sufficient energy transfer, the focalization conditions were usually very constraining as reported by Tsong [32].

During the 1990s, Tsong [32] and Cerezo [4] proposed to solve these problems by using ultra-short laser pulses. According to them, the electrical field of the electromagnetic wave for sub-picosecond laser pulses could trigger the evaporation by acting as an ultrashort HV pulse. For femtosecond laser pulses, a field of 10^9 V m⁻¹ can easily be generated even for low focalizations. Such high optical field is of the same magnitude as the evaporation field for atoms. Moreover, using fs pulses, strong focalizations are not necessary to evaporate atoms so that reproducible measurements could be expected.

At the beginning of 2000, the first results were reported using ultra-fast laser pulses. These results gave good spatial resolution images, as shown in Fig. 1(b), where the crystallographic structure of tungsten can clearly be seen, with good mass resolution, which was only limited by the detector's time response, as shown in Fig. 1(c). These encouraging results showed that the evaporation of the surface atoms was fully controlled and that the use of laser pulses did not lead to the tip's ablation. Moreover, the clear observation of the crystallographic structure was correlated to the absence of any important vibration of the crystal lattice such as the one expected for nanosecond pulses [28] due to the sample's heating. Moreover, good mass resolution proved that, if the evaporation was thermally assisted, the tip's cooling was below 1 ns contrary to the calculated predictions of Lee [31] and Liu et al. [29].

New experiments and new models were thus developed to determine the main evaporation mechanism of surface atoms from metallic and nonmetallic tip.

3. Metallic tips

3.1. Thermal effects

To evaluate the cooling time of a W tip after the interaction with a fs laser, Vurpillot et al. [33] set up a pump probe experiment with a laser pulse pump to heat the sample and an electric pulse as the probe. Studying the evaporation rate generated by the pulse probe versus its delay to the pump, they reported the time evolution of the tip's temperature as shown in Fig. 3. To adjust this data, they considered the cooling process of an infinite cylinder.

The tip is illuminated by a gaussian laser beam of width w so that it is relevant to consider that the temperature increase follows the same spatial profile so that

$$T(t = 0, x) = T_0 + T_{rise} \cdot e^{-x/2w^2} \quad (4)$$

along the tip axis: x . The time $t=0$ corresponds to the end of the thermalization of the electrons with the lattice (a few ps after the pulse). The system's temperature then follows a simple thermal diffusion behavior as predicted by Fourier's law with a thermal diffusivity coefficient D . The temperature at the tip's end is thus

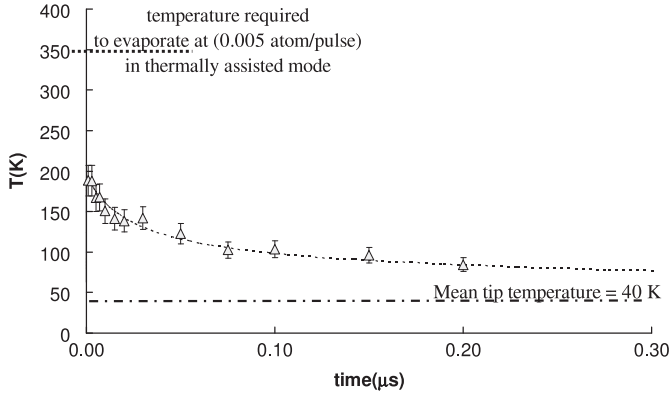


Fig. 3. Tip's end temperature versus time delay after the laser pulse.

described by

$$T(t, x=0) = T_0 + \frac{T_{rise}}{\sqrt{1 + 2\frac{t}{\tau_{cooling}}}} \quad (5)$$

where

$$\tau_{cooling} = w^2/D \quad (6)$$

is the tip's cooling time.

Using Eq. (5) to adjust the data in Fig. 3, the parameters T_{rise} and $\tau_{cooling}$ were evaluated. The initial tip's temperature was insufficient to trigger evaporation and the cooling time was fast corresponding to a heated zone of about $w = 1.5 \mu\text{m}$ which was much smaller than the laser spot's size of about $800 \mu\text{m}$. This simple heat propagation model however relied on the following approximations:

- the tip is heated homogeneously across its cross-section as suggested by Tsong, Liu et al. [30].
- the heated zone corresponds to the size of the laser spot. This hypothesis was based on all the studies concerning the heating and dilatation of laser illuminated tips in near field microscopy.
- the tip has been approximated as a cylindrical wire therefore the heated zone determined from the cooling time is underestimated.
- it is assumed that the cooling dynamics at times shorter than 1 ns could be deduced by continuity from the results obtained for longer times.

In 2005, when this experiment was reported, no experimental evidences invalidated these hypotheses and approximations. Hence, the model of thermal assisted evaporation was considered unable to explain the ultra short laser assisted evaporation and other models were developed.

3.2. Field effect

One possible mechanism to explain the observed field evaporation under ultra-fast laser pulsing could be the lowering of the surface potential barrier by the laser field itself [34]. With the strong peak intensity of the ultra-fast laser, sufficient amplitude values of the optical electric field are obtained. However, the laser field oscillates at optical frequencies (10^{15} Hz) so that the period of field oscillation, τ_{laser} , is short (about 1 fs ($\tau_{laser} \ll \tau_{evap}$)). This means that the potential atomic barrier oscillates too fast, compared to the typical evaporation time, τ_{evap} .

A new physical mechanism was proposed, based on the non-linear optical properties of surfaces [35]: the optical rectification

(OR) effect at metal surfaces [36] which corresponds to the generation of an ultra fast electrical pulse at the surface of the sample when it is illuminated by an ultra fast laser [37,38]. The optical rectification is based on nonlinear second order processes which occur in all non-centro-symmetric materials and at the surface of metals where the electronic density of states exhibits a discontinuity resulting in strong anharmonic and non-linear effects [39,40].

Considering the anharmonic potential, for a low excitation, the electrons motion follows the laser field oscillation; however, for a high excitations new frequency can be generated. In the case of the optical rectification, a standing field can be generated during the laser pulse. Theoretically the expression of the amplitude of the field generated by optical rectification can be obtained:

$$F_{OR} = -\chi_{S,zzz}^{(2)} L_{eff}^2 I_0 / (l_p \epsilon_0 c), \quad (7)$$

with L_{eff} being the enhancement factor depending on the laser polarization and tip shape [41], $\chi_{S,zzz}^{(2)}$ is the relevant second-order susceptibility tensor for OR, $l_p = 3 \text{ \AA}$ which is the characteristic thickness of the interfacial layer in which the second-order surface polarization is nonvanishing and c the speed of light in vacuum. I_0 is the laser intensity and ϵ_0 the vacuum permittivity.

Experimental evidence of the presence of this rectified field can be obtained by investigating the field emission flux dependance on the laser intensity. In Eq. (1) one must add to the standing field (F_{DC}) the rectification field (F_{OR}): $F_T = F_{DC} + |F_{OR}|$. Hence, from Eq. (2), in the first approximation, a linear dependence of the ion flux ϕ with the laser intensity must occur on a semi-logarithm scale. This linear dependence was pointed out for a W tip for two different base temperature values of the tip (20 K and 100 K), as reported in Fig. 4.

However, this experimental behavior can also be understood considering a linear increase of the tip temperature with the laser intensity: $T = T_0 + \eta I$, as reported in Fig. 4 by the solid line.

To identify the dominant evaporation mechanism, an autocorrelation setup was used to measure the evaporation time [42]. In the case of a field evaporation assisted by the optical rectification effect, the evaporation time is extremely short, as short as the laser pulse. In contrast, for thermal evaporation, the evaporation time is related to the cooling process of the sample which is significantly longer than the laser pulse duration.

Focusing two laser pulses with a variable delay on the metallic tip, a very high evaporation rate was reported for a delay shorter than the pulse duration. Hence to evaporate at a constant rate, the voltage applied to the tip decreases, as reported in Fig. 5. This

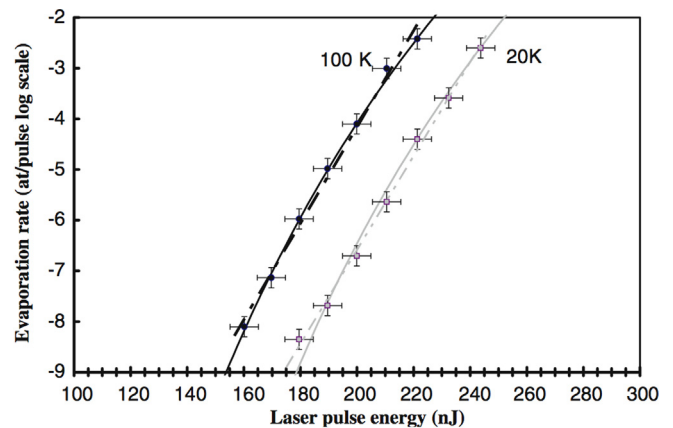


Fig. 4. Evaporation rate measurements for a tungsten tip submitted to an ultra-fast laser illumination. The same measurement was performed at 20 K (grey dots) and at 100 K (black dots). The two sets of curves can be fitted by either the OR model (dashed line) or thermal model (solid line).

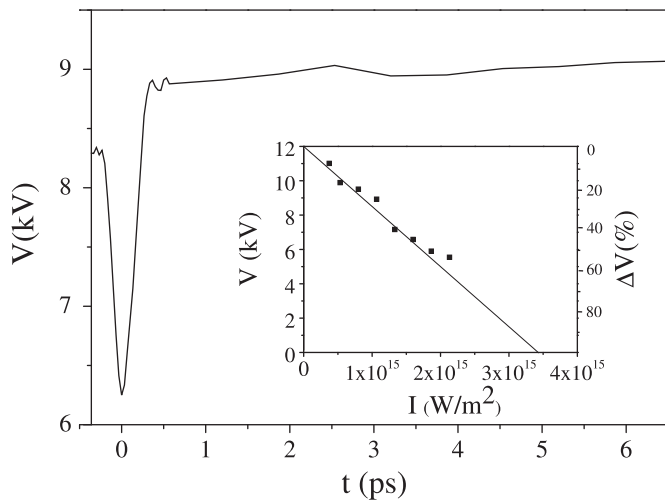


Fig. 5. Evaporation voltage as a function of the delay between two laser pulses for an Al tip.

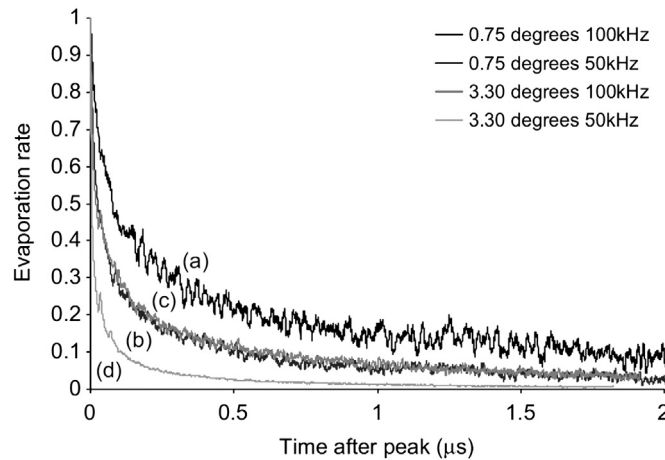


Fig. 6. TOF spectrum of Fe peak from a stainless-steel tip from Ref. [43].

behavior corresponds well to an ultra-fast ion ejection as predicted by the optical rectification effect.

However, the results reported on metals having poor thermal conductivity, such as stainless-steels, show thermal-assisted evaporation [43]. Indeed, when stainless-steels are analyzed in LA-APT, the peak reported in the time of flight (TOF) spectrum are asymmetric (as shown in Fig. 6). This asymmetry corresponds to a long emission, several microseconds after the interaction with the laser pulse. Cerezo et al. [43] showed that the evaporation time dependent on the tip shape (cone angle) and repetition rate of the laser.

Moreover, for W, having a good thermal diffusivity, the migration of surface atoms was reported, related to a loss of spatial resolution in the image reconstruction when the laser intensity used for the evaporation was very high [44]. However, if the evaporation is thermally assisted, the temperature estimated by the pump-probe experiment, reported in Fig. 3 is too low to allow evaporation.

Probably, during the first nanosecond, after the interaction with the laser pulse, a fast cooling, from the illuminated zone to the dark one, homogenize the temperature on the transverse section of the tip. This interpretation was supported by the experimental observation reported by Sha et al. [45]. They observed inhomogeneous evaporation behavior in a stainless steel tip having a radius

of $R=120$ nm analyzed using a green laser ($\lambda=568$ nm) with a pulse duration of 12 ps. The evaporation happens principally from the illuminated side, causing a change in the tip shape which loses the hemispherical shape. This inhomogeneity in the evaporation can be due to the decrease of the diffraction effects (note that the ratio $\lambda/R=4$). However, same evaporation behavior was reported also on smaller radius tips ($R=40$ nm) [46]. This indicates that the hypothesis of strong diffraction of the light at the tip apex and the following homogenous illumination of the apex was wrong. This hypothesis, developed in 1980s, was one of the fundamental hypothesis for all the theory of heating and cooling of the specimen. If the illumination of the apex is inhomogeneous, a fast cooling process becomes possible considering the heat propagation into the transverse direction of the tip.

To get more information on the cooling process of the tip on a time scale shorter than 1 ns, an autocorrelation setup was used, looking at the evaporation rate of the tip for delays between 10 ps to 1 ns, covering the unexplored temporal interval [47].

Fig. 7 shows the evaporation rate, $\varphi_{at/imp}$, as a function of the delay, τ_{pp} , between the two laser pulses.

If the absorption of the tip does not change after the interaction with the first laser pulse, the apex temperature is equal to the sum of temperature rise due to each laser pulse:

$$T_{pp}(t, \tau_{pp}) = T_{pump}(t) + T_{probe}(t - \tau_{pp}) + T_0 \quad (8)$$

Because $T_{pump}(t)$ and $T_{probe}(t - \tau_{pp})$ caring with time according to Eq. (5), a numerical method is used to determine the parameters of the fit reported in Fig. 7. A good agreement with numerical results is obtained for $\tau_{cooling} = 550 \pm 200$ ps and $T_{rise} = 260 \pm 60$ K, corresponding to the rise temperature due to only one laser pulse [47].

This temperature rise is enough to allow the thermally assisted evaporation of the sample. To exclude any nonthermal contribution to the evaporation, the autocorrelation measurements at short delay time, as reported in Fig. 5, were reproduced for a metallic glass and a tungsten tip. The width of the peak at zero delay is always the same, indicating that it corresponds to the constructive interference between the two laser pulses and not to a fast emission [48].

Hence the heating and cooling process of the tip explain well the evaporation mechanism of metals in LA-APT. But one question still remained unanswered: a cooling time of 550 ps, as reported on the tungsten tip, is compatible with a heated zone of about 200 nm, from Eq. (6). This zone is larger than the transverse dimension of the tip (150 nm), hence the fast cooling process cannot be related to a heat diffusion along the transverse section. Moreover this heated zone is smaller than the illuminated zone.

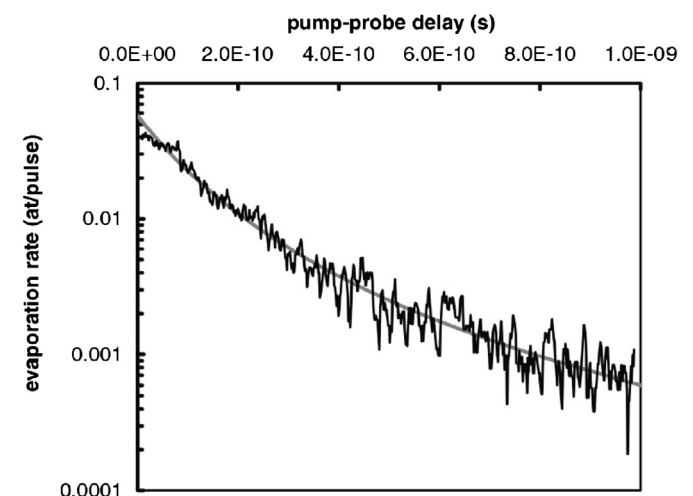


Fig. 7. Evaporation rate as a function of the delay between the two laser pulses.

What is the physical origin of this confinement of the absorption and heating? Only the study of the absorption properties of a nanometric tip can help to answer this question.

3.3. Absorption properties of a metallic, nanometric tip

To take into account the actual tip geometry and its optical properties, absorption 3D maps are computed by finite-difference time domain (FDTD) with a commercial software from Lumerical. In this model, the tip is represented as a cone terminated by a hemispheric cap. It is placed in the simulated space and surrounded by perfectly matched layer avoiding any field reflection. For all wavelengths, the material properties are taken into account by using the dielectric constants taken from Ref. [49].

The computation of the divergence of the Poynting vector leads to the 3D maps presented in Fig. 8 which were calculated for Al at $\lambda = 355$ nm and $\lambda = 1200$ nm and a laser linear polarization parallel to the tip axis (axial polarization). First, spatial oscillations of the absorption with a period equal to λ are observed. Only the illuminated side is reported because any absorption is visible on the opposite side.

In order to evaluate the temperature rise along the tip axis, absorption density profiles along Z axis are presented in Fig. 9. Only the end of the tip is heated and a few micrometers away from the apex, the absorbed energy rapidly decays to zero. In addition, for laser wavelengths longer than 500 nm, the first absorption

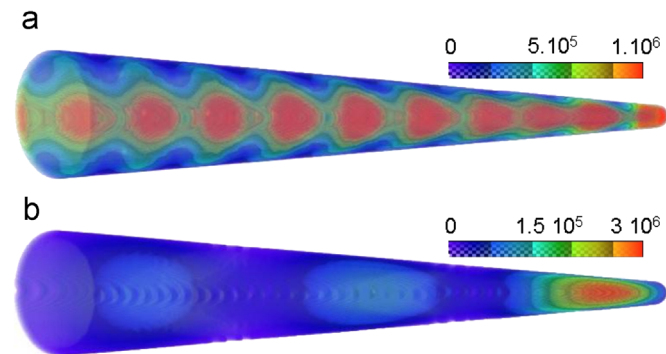


Fig. 8. Absorption maps calculated by FDTD on the illuminated side of the Al tip for axial polarization, at (a) $\lambda = 355$ nm and at (b) $\lambda = 1200$ nm. The color bar is in (W m^{-2}) and corresponds to the power absorption density for an incoming intensity of 1 W m^{-2} .

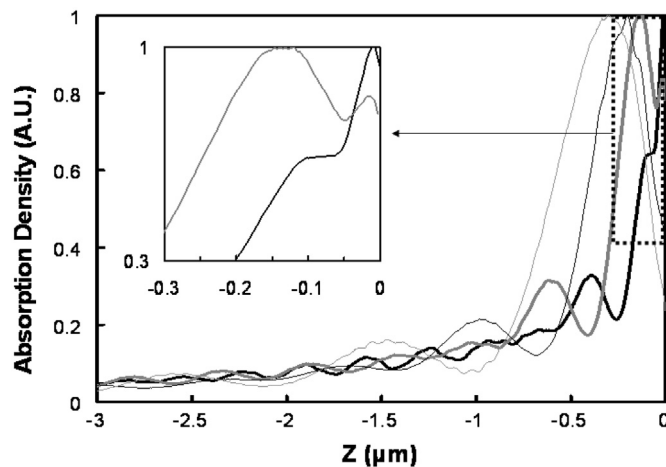


Fig. 9. Normalized absorption density profile along the tip axis computed with previous maps for $\lambda = 360$ nm (black), $\lambda = 515$ nm (gray- thick line), $\lambda = 800$ nm (gray- thin line), and $\lambda = 1200$ nm (light gray).

maximum is located at $\lambda/4$ from the tip apex as shown in Fig. 9. It can be noticed that the shape of absorption maps is the same for steel and aluminum. Only the absolute amplitude of the absorption changes.

These results explain well the small heated zone measured by the autocorrelation set-up.

In order to show experimentally this absorption confinement and its dependence on the laser wavelength and polarization, the evaporation behavior of a stainless steel tip was studied. Due to the low thermal conductivity of the stainless steel, the cooling time of the tip is long, hence the evaporation time is longer than the time detector accuracy. Due to the exponential decay of the evaporation rate (Eq. (2)), most of the atoms are evaporated in the very first moments of the cooling process. Let us define the evaporation time τ_{evap} as the time at which the evaporation rate has decreased to one tenth. Inserting Eq. (5) in Eq. (2), and taking $(k_B T_{\text{max}})/Q_n = 5\%$ from Ref. [47], τ_{evap} is given by

$$\tau_{\text{evap}} = \ln(10) \times \frac{k_B T_{\text{max}}}{Q_n} \times \frac{w^2}{D} \approx 0.1 \frac{w^2}{D}. \quad (9)$$

Hence, measuring the evaporation time using APT, an estimate of the size of the heated zone can be obtained and a study of the absorption confinement can be made.

For a stainless steel tip ($\text{Fe}_{0.7}\text{Cr}_{0.19}\text{Ni}_{0.07}\text{Si}_{0.03}$) having a thermal diffusivity of $\alpha_{\text{inox}} \approx 5 \times 10^{-6} \text{ m}^2 \text{ s}^{-1}$ the evaporation time τ_{evap} strongly depends on the laser wavelength: $\tau_{\text{evap}} \approx 2$ ns for $\lambda = 320$ nm and 20 ns for $\lambda = 1200$ nm, corresponding to a heated zone of $w \approx 300$ nm and ≈ 1000 nm, respectively.

Unexpectedly, the peaks present a slower rising edge at longer wavelengths. Following the infinite cylinder model the heated zone corresponds to the width of a Gaussian temperature distribution centered on the tip apex. If, due to the absorption process, the maximum temperature is not located on the tip end but somewhere further on the shank, the maximum evaporation rate is not reached just after the laser pulse, but a time τ_{rise} later, due to the thermal diffusivity. From Fig. 10, τ_{rise} is calculated to be 5 ns for $\lambda = 1200$ nm and to 2.8 ns for $\lambda = 750$ nm. The position Z_0 of this maximum temperature can be evaluated using the law of heat diffusivity, $Z_0 = \sqrt{D_{\text{steel}} \tau_{\text{rise}}}$. For $\lambda = 1200$ nm, $Z_0 \approx 220$ nm and for $\lambda = 750$ nm, $Z_0 \approx 170$ nm, i.e. small fractions of the value of the wavelength.

These experimental results are already in good agreement with the prediction of the numerically calculated absorption maps (Fig. 8). But these maps give information on the free electron absorption, whereas the evaporation rate is related to the lattice temperature not to the electronic temperature. A complete 3D thermal model is necessary to evaluate the lattice temperature and its evolution.

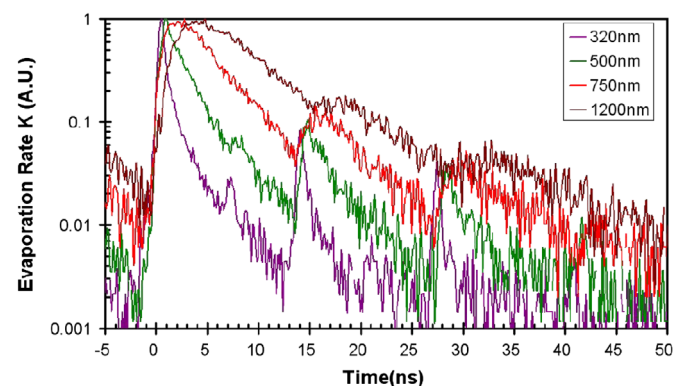


Fig. 10. Evaporation rate as function of time obtained from a stainless steel tip, for different wavelengths in axial polarization.

3.3.1. 3D thermal model

The laser energy is absorbed locally by electrons, which transport the energy by ballistic motion with a speed equal to the Fermi speed. To take into account this ballistic motion, a ballistic penetration depth (ϵ_{bal}) is introduced in absorption maps [54]. Temporal transient temperature distributions in a nanometric tip subjected to ultrashort laser pulses were obtained from a three-dimensional (3D) analysis. The parabolic two temperature model [55] simplified by neglecting lattice conduction, is used to model heating by a heat source with Gaussian temporal distribution. Spatial distribution is given by the absorption map as described. Lattice conduction was neglected because, in metals, thermal conductivity is governed by electrons [56,57]. The 3D thermal model can be used to explain the localized preferential evaporation observed by Sha et al. [45] on a steel tip. Using a ballistic depth coefficient of 14 nm and an electronic conductivity of $19.6 \text{ J m}^{-1} \text{ s}^{-1} \text{ K}^{-1}$, the temperature evolution on different parts of the tip apex can be calculated. As shown in Fig. 11, the temperature evolution depends strongly on the position of the tip surface. The side illuminated by the laser beam reaches 280 K in less than 1 ps, however, the dark side reaches the maximum temperature of 230 K only 100 ps after the laser-tip interaction. This delay is due to the 3D heat propagation from the illuminated side to the dark one. In Fig. 11 the evaporation rate corresponding to these two apex zones was calculated using an activation energy value of 0.4 eV. The evaporation rate is ten times higher for the illuminated side, indicating this side of the tip ejects more ions (preferential evaporation) and the radius increases, as reported in Ref. [45].

3.4. Conclusions

The dominant evaporation mechanism for metallic tip in LA-APT is the thermally assisted evaporation. After the interaction with the laser, the tip temperature increases and surface atoms are evaporated as ions by the thermal activation process. Moreover, the diffraction effects allow the confinement of the absorption at the apex of the tip on the illuminated side. The size of the

absorption zone is smaller than the laser spot size and almost equal to the laser wavelength. However, when surface plasmons of the nano-sphere which terminates the tip are excited, absorption is homogenous. In all these cases, the absorption zone is very small and these corresponds to a small heated zone, which allows a fast cooling of the tip apex and a fast thermally assisted emission of surface atoms. Moreover, when a fs laser is used, the electrons can absorb all the photon energy fast, hence their temperature can be very high. These hot electrons can diffuse rapidly and these ballistic diffusion effect is important in the lattice heating effect and is at the origin of the spatial homogeneity (or inhomogeneity) of the evaporation.

4. Silicon tips

Silicon is a material widely analyzed in APT and LA-APT with a wide range of applications in microelectronic domain. First analysis of silicon reported by Tsong and Kellogg [9] showed that the analysis conditions in LA-APT were very critical. For example, the presence of hydrogen in the chamber could lead to evaporation of a large amount of SiH ions, or, at high laser power, silicon is evaporated as clusters. Using ns or several hundred of ps laser pulses in the near ultraviolet (UV) only 20% of atoms was evaporated as single ion (Si^{1+} or Si^{2+}). However, the energy distribution of these ions suggested the possibility of evaporation assisted by photo-ionization, corresponding to the absorption of one or two photons directly by the surface atoms. This technique was not used due to difficulties associated with the strong focus of laser on the tip which effects measurement precision. Another issue is finding appropriate analysis conditions for each sample to avoid cluster evaporation [32].

First analysis of Si tips using fs laser pulses, showed well controlled field evaporation with only atomic species and almost no clusters detected. Three evaporation regimes were reported with changing the laser intensity [58]:

- at low laser intensity, a regime of resonant photo-ionization
- at middle laser intensity, a regime of fast and well controlled evaporation
- at high intensity, a very slow evaporation follows a first fast evaporation

Intrinsic silicon or very lightly doped silicon has a low number of mobile charge carriers at the analysis temperature (50 K) and thus cannot screen the electric field at the surface. Hence, the field penetration depth can be of several nanometers and can induce evaporation of clusters. In the presence of mobile charges, the surface field causes a curvature of the electronic bands at a depth of about 1 nm. This phenomenon has been well-studied by Tsong to understand why illuminating a silicon tip results in good FIM images of the surface [19]. To obtain FIM images, the surface has to accommodate electrons of the gas atoms which can tunnel to the tip. This tunneling effect is possible only if some available electronic states exist at the surface. When the surface field is very strong, as in the case of APT, the curvature of the band can lead to a change of the surface properties of the material which becomes almost metallic. Fig. 12 shows that at the surface the valence band is above the Fermi level, so that locally the material is metallic.

Hence, in order to achieve a controlled evaporation of silicon, it is necessary to screen the surface field by mobile charges. These charges can be created by the absorption of photons from the laser and it must thus be ensured that this absorption occurs.

Silicon is an indirect gap semiconductor ($E_g = 1.12 \text{ eV}$) with a low absorption at wavelengths of near infrared (as $\lambda = 1030 \text{ nm}$) or visible (as $\lambda = 515 \text{ nm}$). However, its absorption is strong for

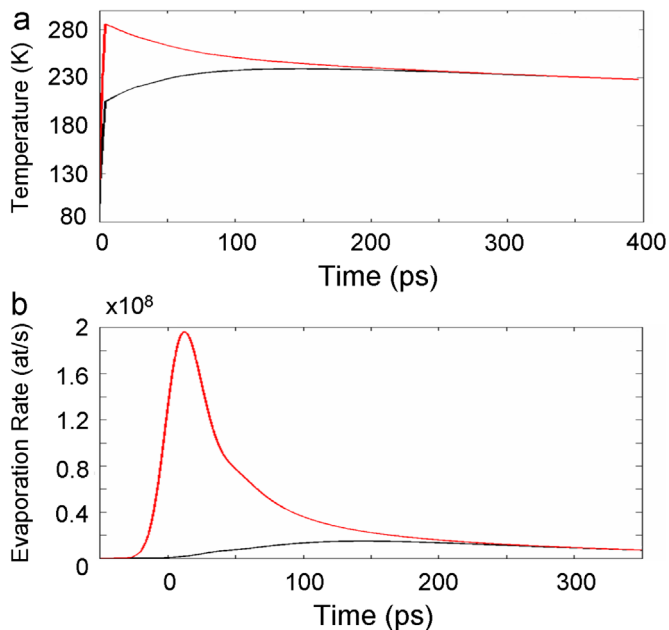


Fig. 11. (a) Temperature evolution and (b) evaporation rate of a steel tip after the interaction with the laser pulse (red line: the illuminated side of the tip; black line: the opposite side). (For interpretation of the references to color in this figure caption, the reader is referred to the web version of this article.)

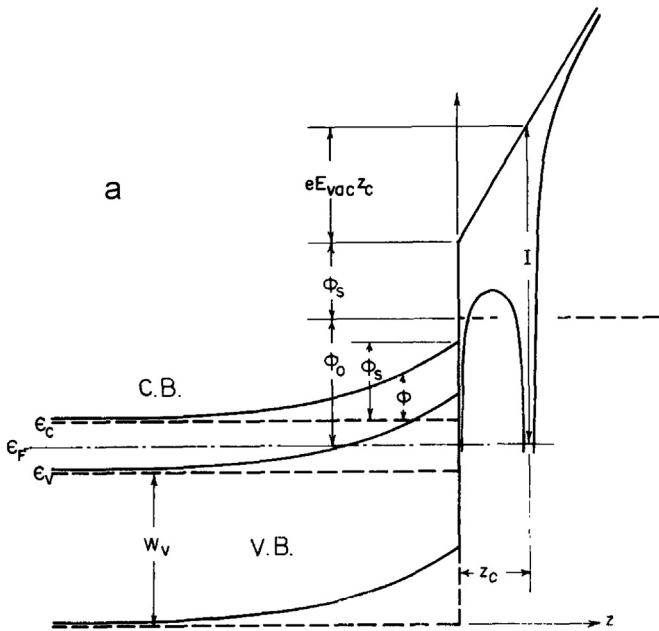


Fig. 12. Band structure of silicon under high electric field.

wavelengths of near UV corresponding to a photon energy higher than direct band-gap of silicon ($E_g^d = 3.4$ eV). Therefore, to generate charges in the silicon it is better to use UV laser, as done by Tsong and Kellogg [9]. However, first analysis reported using ultra fast fs laser was obtained with a near-IR light ($\lambda = 1030$ nm).

4.1. Photo-ionization regime

At very low intensity, a linear dependence of the evaporation rate of Si on the laser intensity was reported. For this regime of photo-ionization, the surface atoms absorb a photon and can thus be ionized. In fact, their lifetime is related to the time necessary to other electrons of the material to neutralize the surface charge. If the material has a band gap, as in the case of all semiconductors, the neutralization time may be of a few ps. Hence ions created by direct absorption of a photon on the surface of the tip are likely to evaporate. The evaporation rate will be proportional to the ionization rate and thus proportional to the laser intensity.

This linear dependence of the evaporation rate on laser illumination was shown experimentally for a laser intensity lower than 1 GW/cm^2 and a wavelength of $\lambda = 1030$ nm [59]. Hence when the incident photon energy is close to the band gap energy of silicon, the photo-ionization process is induced by a single photon absorption (mono photonics process). When the photon energy increases (for $\lambda = 515$ or 343 nm) the evaporation rate is not a linear function of the laser intensity, showing that a multi photon absorption process becomes possible, as evidenced by Tsong [60].

The formation of an ion at the silicon surface by photo ionization is a very fast process and it takes place during the interaction between the laser pulse and the tip. But what happens to those ions after their generation? Are they evaporated instantly or do they stick on the surface of the material? In this case, what is their life time before their evaporation or re-neutralization?

Because the ratio between the number of ions formed at the surface and the ions evaporated is greater than one, ions remain on the surface and are therefore neutralized. Obviously, there is an energy barrier for ions to evaporate and therefore a certain probability of crossing this barrier. The height of this barrier was estimated and the life time of ions deduced, from experimental observations. This life time is equal to the duration of the laser pulse [59].

4.2. Fast evaporation regime

When laser intensity is increased, the photoionization regime is masked by thermally assisted evaporation. As shown in Fig. 13, the flight time spectrum shows two contributions: a slow evaporation which takes place several nanoseconds after the laser pulse due to a slow cooling process and a fast evaporation, faster than the accuracy of the time detector. Using the 1D cooling model reported in Eq. (5), the slow evaporation can be easily fitted using $w = 200$ nm for the size of the heated area and a temperature increase of several hundred degrees Kelvin (about 300 K). Measurements reported in Fig. 13 were obtained with a fs laser in IR ($\lambda = 1030$ nm). An increase in temperature by 300 K after the interaction with the laser can only be due to the relaxation of the energy absorbed by the electrons to the lattice. By a simple energy balance, the energy stored in the system ($C_v T$) must be equal to the energy absorbed ($E_{ph} N_0$ with N_0 the number of charges created in the sample). For $T = 300$ K a charge density of $N_0 = 10^{21} \text{ cm}^{-3}$ is calculated. This density is too high if we take into account the low absorption of Si at this wavelength ($N_0 = \alpha I / h\nu = 10^{16} \text{ cm}^{-3}$, with I the laser illumination, ν its frequency and α the absorption coefficient).

Moreover, changing the laser wavelength does not change the fast evaporation peak, only the duration of the slow evaporation changes (as shown in Fig. 14).

The absorption maps calculated by the FDTD method (see Fig. 15) show a different behavior of the silicon absorption with the wavelength, as expected by its band structure. In the near UV, absorption is a strong surface phenomenon. However, in the visible and near IR regime, absorption presents some maxima inside the volume, due to interference effects of the reflected waves at the tip-vacuum interfaces.

When UV light is used, the evaporation behavior of Si tips is similar to that of metal tips with absorption confined at the surface and an inhomogeneous evaporation (see Fig. 16). Singly-charged ions are evaporate from the illuminated side of the tip and doubly-charged ions from the dark side of the tip, as reported by Koelling et al. [61].

This effect can be easily understood if we assume that the temperature of the tip is higher on the illuminated side than on the opposite side. To evaporate at a constant emission rate, the field needs to be weaker on the illuminated side. This variation of the local field is related to a change in the surface profile of the tip as shown in Fig. 16. However, when the tip is evaporated using a green laser, the evaporation is homogeneous and deformations of the spherical geometry are not observed (Fig. 16(c)). Koelling et al. [61] explain these different evaporation behavior by the

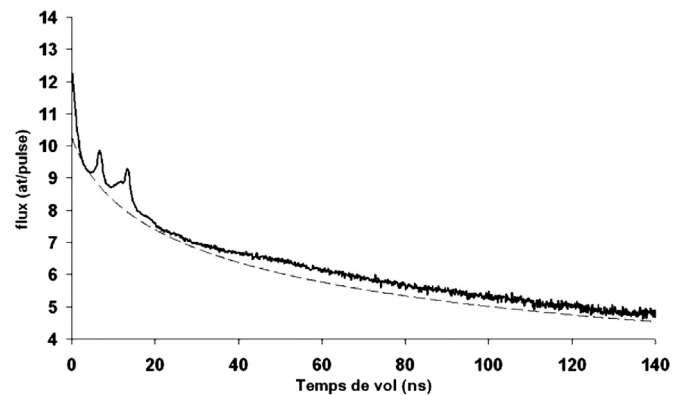


Fig. 13. TOF spectrum on semi-log scale of $^{28}\text{Si}^{2+}$ peak (full line): the two smaller peaks correspond to isotopes $^{29}\text{Si}^{2+}$, $^{30}\text{Si}^{2+}$. Fit using Eq. (5) with $T_{\text{rise}} = 275$ K, $\tau_{\text{cooling}} = 4$ ns (dashed line).

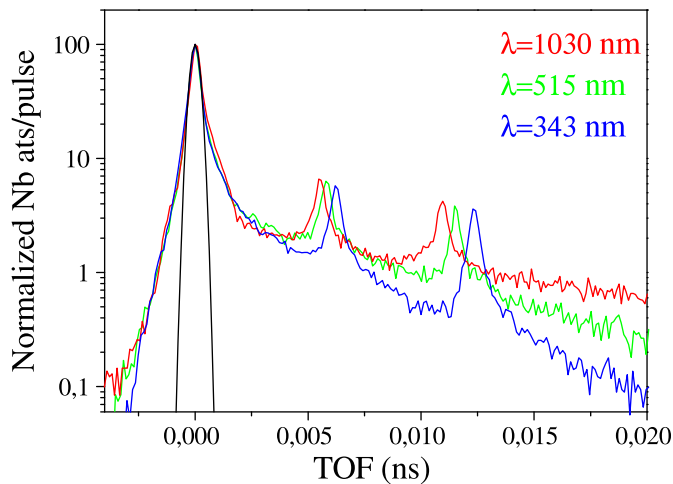


Fig. 14. TOF spectrum on semi-log scale of Si^{2+} peak for different laser wavelengths.

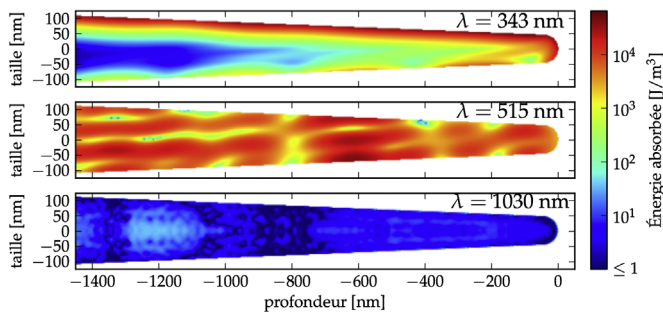


Fig. 15. Absorption maps of Si tip illuminate with (a) UV light $\lambda = 343$ nm, (b) green light $\lambda = 515$ nm and (c) IR light $\lambda = 1030$ nm. (For interpretation of the references to color in this figure caption, the reader is referred to the web version of this article.)

absorption maps obtained using FDTD calculations. As reported in Fig. 15, with a green laser the absorption map presents maxima in the volume which give rise to a homogeneous heating of the tip apex.

However, these absorption maps cannot explain the presence of a fast emission peak for the three wavelengths. As shown in Fig. 14, this peak is identical (same rise time, same decay time, same width) for the three wavelengths. In the case of UV excitation, this peak may be associated with a rapid cooling from the illuminated side to the dark side, but how can we explain this fast evaporation for the other two wavelengths?

Only a localized absorption very close to the apex of the tip could explain this behavior reported experimentally.

It is known that, under intense electric field, the absorption efficiency of silicon for wavelengths close to the gap (in the near IR) can be increased by the Franz-Keldysh effect [62]. In the case of the APT analysis, the surface field is very strong and this effect may be masked by the inversion of surface properties as reported by Tsong [19]. To take into account the role of the electric field on the absorption properties of Si and to calculate the evolution of these properties during the laser pulse, the temporal evolution and the spatial distribution of charges have been calculated [63]. As shown in Fig. 17 few hundred fs after the laser pulse, a high density of holes is generated at the surface and, consequently, the electric field is screened. These calculations can explain why the evaporation of silicon in APT can be well controlled. In reality the field is screened at the surface as in the case of metals. In addition, these results show that a high density of charges is generated at the surface. These free holes can absorb the laser energy. Hence the

absorption coefficient of the surface increases considerably, by several orders of magnitude for $\lambda = 1030$ nm.

As discussed in the previous section on metals, in the case of silicon it is also necessary to link the absorption properties of the surface to the heating and cooling dynamics of the samples to study the temperature evolution and the evaporation dynamics. In silicon, as in semiconductors in general, the energy transfer from the electrons to the lattice is more complex than it is in metals, due to the presence of forbidden energy bands. This can give rise to a new evaporation behavior, as reported in the next section.

4.3. Slow evaporation regime

For intrinsic silicon and n or p doped silicon, a delayed emission is visible when a laser illumination at $\lambda = 1030$ nm is used (see Fig. 18). This evaporation must be correlated to a heating of the tip apex several nanoseconds after the laser pulse. To understand this delayed heating of the sample, the relaxation mechanisms of the energy absorbed by the electrons during the interaction with the laser and the mechanisms to transfer this energy to the lattice have to be analyzed, as reported by Mazumder et al. [64]. Recently, delayed peak in the evaporation rate has also been reported when Si tips are analyzed with a green laser. Presumably, the absorption maps of silicon under high field present the strong absorption at the apex, due to the band-bending at the surface, as well as an absorption deeper in the volume, due to the penetration of the laser wave and its multiple reflections, as shown in Fig. 15. This absorption, which is far from the apex of the tip, can lead to the delayed evaporation of surface atoms.

4.4. Conclusions

Studying the evaporation behavior of silicon, the process of resonant photoionization was reported at low laser fluence. At higher laser fluence, a process of rapid evaporation was observed. This fast evaporation is related to a confinement of absorption at the surface of the tip apex. The absorption at the surface is probably due to the band-bending taking place at the surface because of the strong electric field. This band-bending phenomenon completely changes the optical properties of silicon surface.

A complete model in the real 3D geometry of the tip is necessary to model the tip absorption realistically under high electric field and the following heating and cooling process of the lattice. At the same time, new experimental results are needed to validate this model.

5. Oxide tips

In the 80s, few LA-APT analysis were reported on oxides. Indeed, semiconductors monopolized the interest of researchers considering their wide range of applications in microelectronics. Only Kellogg [65] analyzed two insulators using LA-APT: pyrex and fused quartz. To obtain evaporation, the tips were covered by a metal layer of Cr of 50 nm after a smaller thickness of 5 nm was not successful. This metal layer, according to Kellogg, plays several roles: it allows to bring the potential to the tip apex, otherwise, considering the dielectric nature of the tip, a sharp voltage drop was expected between the base and the apex of the sample. Moreover, the metallic layer also allows the absorption of laser energy. Kellogg used a UV laser ($\lambda = 337$ nm), and at this wavelength, the absorption of the two glasses is very low. Kellogg justified the need for a 50 nm thick metal explaining that a thinner layer is not enough to absorb light. Finally, the metal layer also allows fast heat dissipation necessary to obtain well resolved mass spectra. In the analyses reported by Kellogg a lot of molecular ions

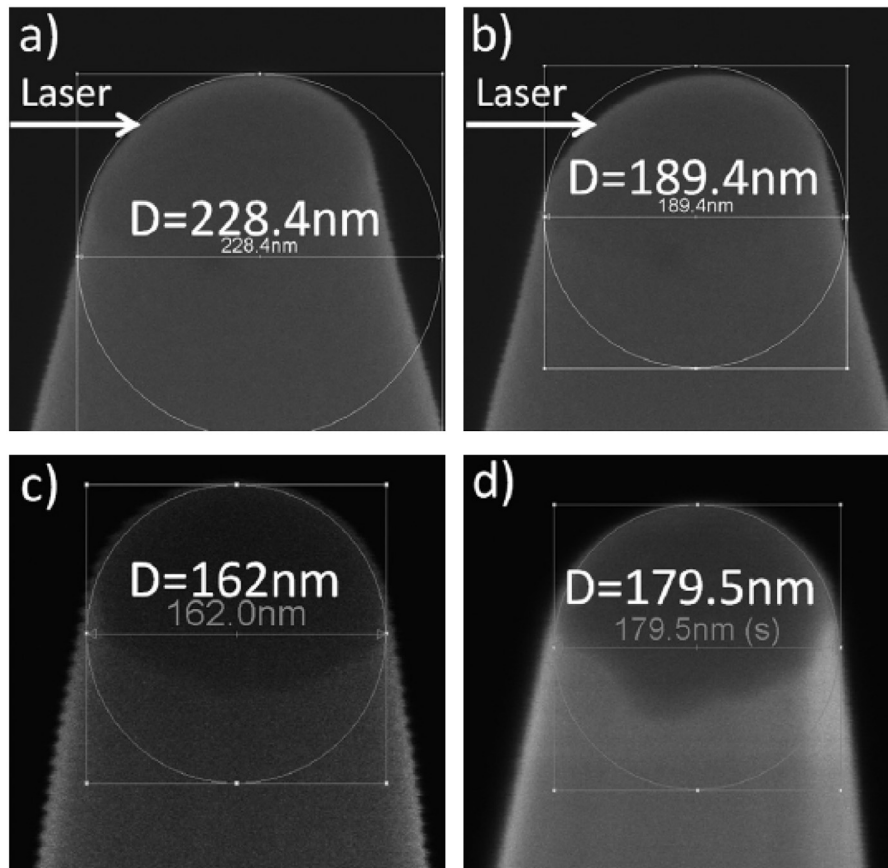


Fig. 16. SEM images of a silicon tip after analysis with (a), (b) a UV-laser, (c) a green-laser, and (d) field ion microscopy [61].

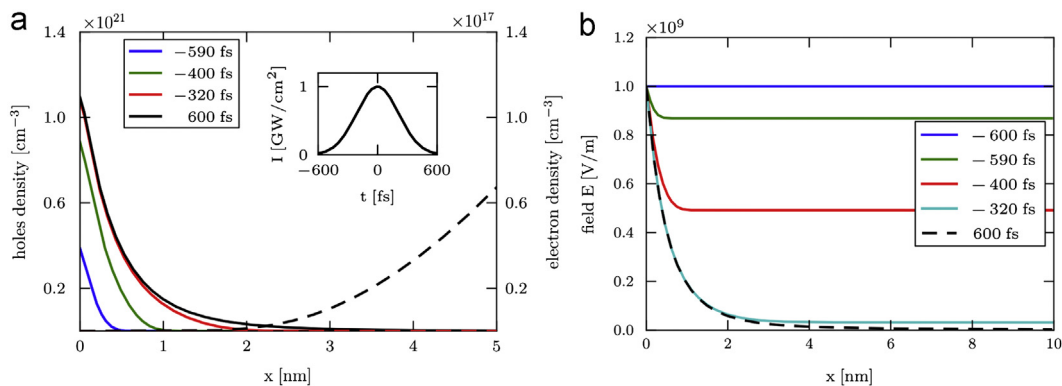


Fig. 17. Depth profile of holes density (a) electric field and (b) at difference delays after the laser pulses.

CrO are detected. To overcome the use of this metallic layer, Kellogg suggested the use of a laser whose energy can be absorbed directly by the oxide. Unfortunately, the energy gap of oxides is large, more than 5 eV, and the photon energy of the laser in the near UV is below this gap energy.

Of course, using ultra-short laser, the nonlinear absorption processes (absorption of two or three photons) become more likely and it becomes possible to excite large gap oxides with a UV laser or even visible-light laser.

In confirmation, the work of Stoian et al. [66] showed that it is possible to ablate large gap oxides by a nonthermal process such as ‘Coulomb explosion’ by exciting with IR, fs laser. Hence, using fs

laser, the difficulties in LA-APT analysis of wide-gap oxides can be overcome.

Naturally, at the beginning only thin layers of oxide were analyzed. Several groups around the world are working on the analysis of thin oxide layers in tunnel barriers. Some barriers, such as Al_2O_3 between $\text{Ni}_{79}\text{Fe}_{21}$ electrodes can be easily analyzed using an electric APT [67]. Others, such as MgO barriers between Fe electrodes, systematically break when the thickness of the oxide layer is greater than 2 nm.

The first analysis of two layers of 4 nm of MgO between Fe electrodes was reported in 2005 using LA-APT [68]. Hence, with laser pulses it became possible to study thicker oxide layers and

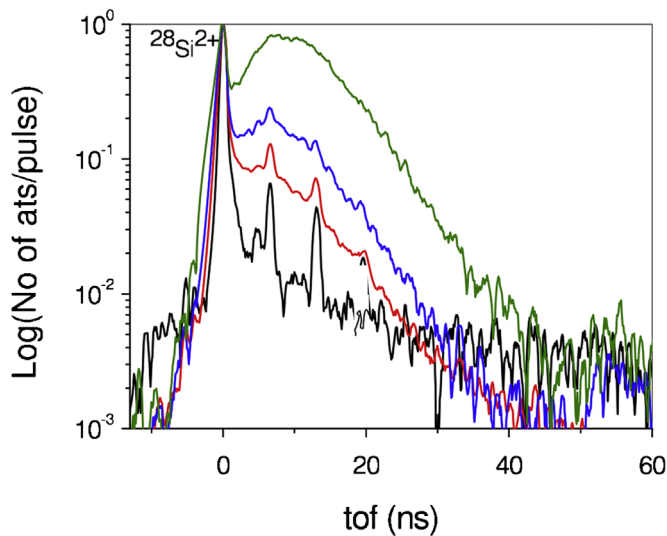


Fig. 18. TOF spectra of Si^{2+} (a) for IR laser. Black line $I=0.2 \text{ GW/cm}^2$, red $I=1.2 \text{ GW/cm}^2$, blue $I=2.2 \text{ GW/cm}^2$, and green $I=5.7 \text{ GW/cm}^2$, respectively. (For interpretation of the references to color in this figure caption, the reader is referred to the web version of this article.)

analyze, at the nanoscale, the interface oxide/metal whose roughness strongly influences the properties of tunnel barriers.

5.1. Thin layer of MgO

For thin oxides between two metallic layers, the evaporation of the oxide was supposed to be totally induced by the evaporation behavior of the metallic layer under the laser illumination. Therefore ultra-fast thermal evaporation depending on laser wavelength, polarization and intensity (typical signature of metals) was expected.

4 nm MgO layers was analyzed using green light ($\lambda = 532 \text{ nm}$, $E_{ph} = 2.4 \text{ eV}$) and UV light ($\lambda = 343 \text{ nm}$, $E_{ph} = 3.6 \text{ eV}$) [69]. However, MgO is transparent to these two wavelengths because its band gap is of about 7.8 eV. The absorption should therefore take place mainly in the Fe layers. Moreover, the MgO has approximately the same thermal diffusivity as Fe, hence for all the evaporated species (Fe^{2+} , Mg^{2+} , MgO^{1+}), the same shape of the time of flight spectrum was expected.

In fact, using green laser, the TOF spectrum of Mg^{2+} ions is different from the TOF spectrum of Fe^{2+} ions collected in the first or in the second metallic layer, as reported in Fig. 19(a).

In particular, the spectra of Fe ions show a very long rise time (several ns) due to the absorption of laser energy away from the tip apex (at a distance of approximately $\lambda/4$ from the apex). The heat generated locally by the electron-phonon coupling process, spreads slowly to the apex of the tip. The evaporation rate increases following the slow heating process of the tip apex. However, the TOF spectrum of Mg ions has an extremely fast rise time, shorter than the accuracy of the time detector (about 500 ps).

Hence, when the MgO is at the surface, the absorption of the laser energy is located closer to the apex, probably at the surface.

When an UV laser is used, the TOF spectra have the same structure for all three layers Fe/MgO/Fe, as shown in Fig. 19 (b). Indeed, using UV light, the Fe layer absorbs light at the apex, hence its evaporation behavior is similar to that of the MgO layer.

These experimental observations clearly show that the dielectric layer can absorb photons whose energy is much smaller than the band gap of the dielectric layer when this layer is at the surface. The band-bending under high electric field can induce the

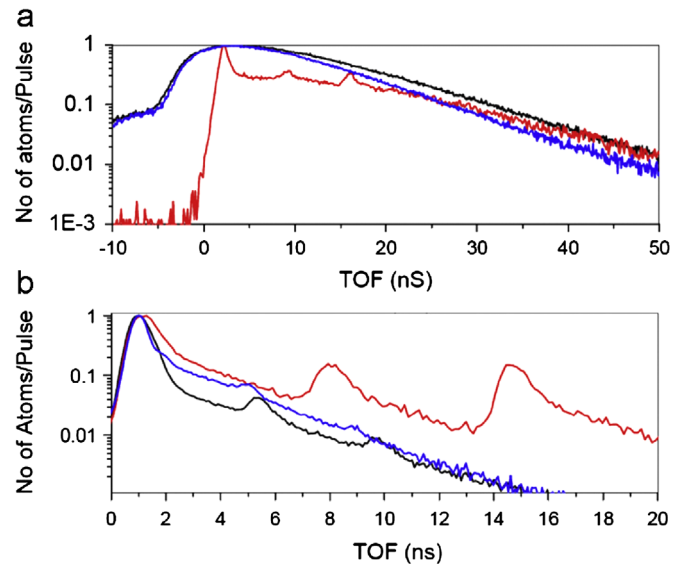


Fig. 19. TOF spectrum of Mg^{2+} ions (red line) and Fe^{2+} ions from the first layer (black line) and the second layer (blue line) (a) analyzed using green laser ($\lambda = 515 \text{ nm}$) and (b) UV laser ($\lambda = 343 \text{ nm}$). (For interpretation of the references to color in this figure caption, the reader is referred to the web version of this article.)

variation of the surface gap which allows the absorption of low-energy photon at the apex.

For thicker layers of MgO, the influence of metallic electrodes on the evaporation of the dielectric layer was supposed to be lower. Initially we were looking for a 'critical' thickness of MgO beyond which analysis becomes unsuccessful. Indeed, by increasing the thickness of the oxide layer, the surface electric field should strongly decrease due to its penetration into the oxide layer. Hence, a high heating of the metal layer would be necessary to evaporate the oxide. Then an uncontrolled evaporation of oxide in clusters was expected.

Actually, the spectra of thick MgO layer of 32 nm are identical to those carried on thin layers of 4 nm with green and UV light, the laser energies are equivalent and evaporation happens atom by atom [69].

It is therefore clear that the layer of MgO is involved in the absorption of the laser light, and this absorption is localized at the tip apex. This localization leads to very narrow TOF peaks of Mg^{2+} whatever the laser wavelength used. Moreover, this absorption also allows the screening of the static electric field and thereby the controlled evaporation of oxide layers.

5.2. Bulk oxides

The first LA-APT analysis of bulk oxide was reported by Chen et al. [70] on a ceramic nanocomposite, using a fs laser in the UV range. This work opened the application of LA-APT to oxides.

The group of Prof. Hono from the University of Tsukuba in Japan started analyzing other wide band gap oxides (such as MgO, ZnO) to understand their evaporation mechanisms. According to the results reported by this group, the use of a UV laser is necessary to analyze dielectrics. The UV laser is more efficient than green laser with an improved mass resolution and higher rate of success [70–73].

At the same time Marquis et al. [74] showed that alumina can be analyzed using green or UV laser and the rate of success and the mass resolution are comparable. To explain why it was possible to analyze the alumina with photon having an energy lower than the band gap energy, which is of about 8 eV, the authors proposed to take into account the modification of the band structure of the

surface, as described by ab initio calculations. Also the amorphization of the surface during the preparation of tip by Focused Ion Beam (FIB) milling can change the surface gap which would be of about 2.5 eV, lower than the photon energy.

From these initial studies it seems clear that the oxide evaporation is a surface phenomenon because optical properties of the surface are significantly different from that of the bulk oxides. Moreover, Chen et al. [75] showed that surface field, at the surface of MgO, increases up to that expected for a metal tip during illumination. But how does this absorption occur if the gap of the material is very high? Moreover, are the absorption by the surface defects sufficient to generate a density of free charges which can screen the field?

Tsukuba et al. [76] propose an evaporation mechanism assisted by the accumulation of holes at the surface of MgO. Using ab-initio calculations they show that, if holes are present at the surface, the evaporation barrier is greatly reduced. Thus, if the surface atoms absorb a photon, holes are created at the surface and Mg^{2+} ions can then be evaporated by photoionization. The physical origin of the surface absorption remains unexplained in any case.

These studies on bulk oxides raise same questions as in previous studies of thin or thick layers of MgO. Why does the surface play an essential role in the evaporation of oxides in LA-APT? What are the optical and dielectric properties of surface oxides under high field, considering the screening effect reported experimentally?

5.2.1. Analysis of bulk MgO and TiO_2

MgO has a large band gap (7.8 eV), an ionic bonding and surface vacancy states showing an electronic structure very different from that of the bulk [77,78]. TiO_2 has a smaller band gap (3.4 eV), a covalent bonding and vacancy states close to the bulk states [79,80].

The analyses of these two bulk oxides were performed with the three wavelengths of fs laser: IR, green and UV. Results were obtained only with the UV light on TiO_2 and with UV and green on MgO. When an IR laser is used, even at a high laser intensity no controlled evaporation was obtained. This wavelength dependence can be explained taking into account the presence of oxygen defects which reduces the gap of MgO to about 2.2 eV. However, for TiO_2 the defects do not change enough the gap which is still of 3.1 eV, well above the photon energy in green (2.4 eV).

For low laser intensity, the photo-ionization mechanism can be the dominant evaporation mechanism, in the case of low sample heating. This evaporation by photo-ionization of surface atoms is fast, as long as the duration of the laser pulse, corresponding to a sharp flight time spectra.

The spectrum of TiO_2 obtained at very low intensity, is reproduced in Fig. 20.

Evaporation times are measured as the width of mass peaks at 10% of the maximum (FWTM). As shown in Fig. 20, the FWTM width of TiO^{2+} peak is larger than the mass resolving power of the detector, showing a long tail due to a long emission related to the cooling process of the specimen. A similar behavior was also reported for higher values of the laser intensity. Hence, photo induced evaporation was not reported on these samples.

At higher laser intensity the TOF peaks change structure. As reported in Fig. 22 for TiO_2 and in Fig. 21 for MgO and as reported previously by Marquis on alumina [74], these peaks are the superposition of a fast evaporation and a slower evaporation.

Moreover, in the case of MgO, only the slow process depends on the laser wavelength, as reported in thin MgO [69] and in alumina [74]. Rapid evaporation is probably the result of absorption of the laser energy at the surface very close to the tip apex.

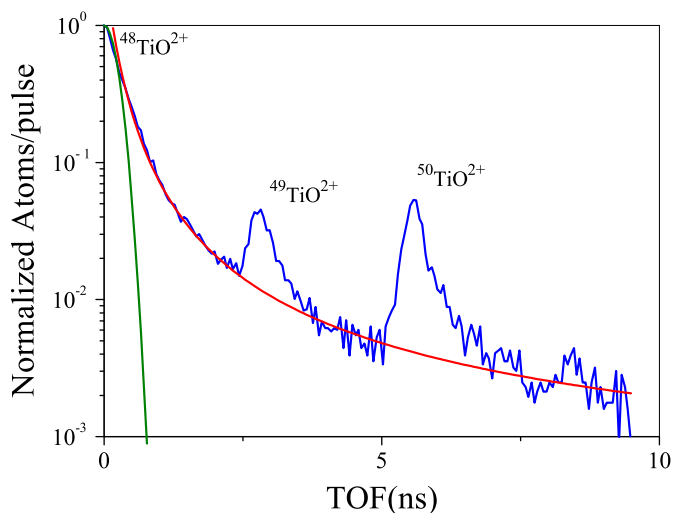


Fig. 20. TiO^{2+} main flight time peak for a laser fluence of 4 J/m^2 (blue line). The red line is obtained from the thermal model. Detector timing accuracy is provided for comparison (green line). (For interpretation of the references to color in this figure caption, the reader is referred to the web version of this article.)

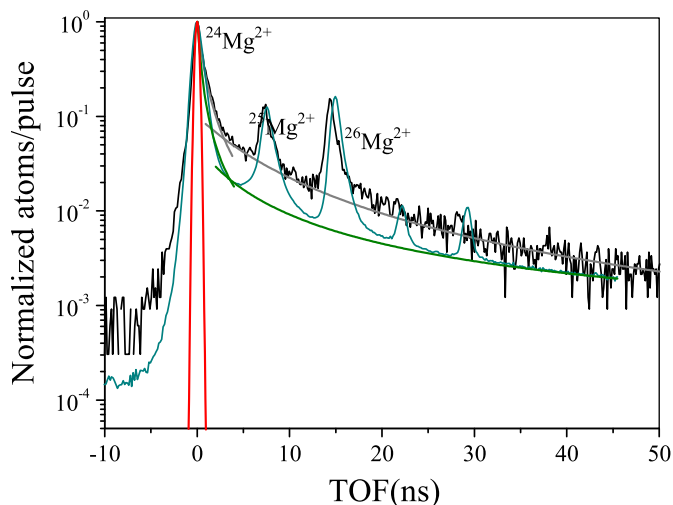


Fig. 21. Flight time spectrum of Mg^{2+} peaks for UV light (olive) and green light (black line). Gray and green lines correspond to the fit using Eq. (5). Fits values for gray line: fast(slow) decay process: $Q_n = 0.1(0.1) \text{ eV}$; $T_{\text{rise}} = 100(100) \text{ K}$ and $\tau = 1(10) \text{ ns}$; For green line: $Q_n = 0.1(0.1) \text{ eV}$; $T_{\text{rise}} = 100(100) \text{ K}$ and $\tau = 2(20) \text{ ns}$. The detector timing accuracy is indicated in red. (For interpretation of the references to color in this figure caption, the reader is referred to the web version of this article.)

Slow evaporation corresponds to the slow cooling along the tip shank after homogenization of the temperature at the apex.

What is the physical origin of this surface absorption at the tip apex?

In the case of MgO, the absorption can be due to the defects (oxygen vacancies), but in the case of TiO_2 for UV light ($E_{\text{ph}} = 3.6 \text{ eV}$) the laser penetration is a few hundred of nanometers, corresponding to an absorption in the total volume. However, if we consider that the oxygen defects can reduce the band gap of 0.3 eV, then the absorption of UV light increases strongly and can explain the confinement of the heating to the surface of the sample.

But, as already discussed for silicon tips, the surface absorption may also be due to the band-bending generated at the surface by the strong electric field. If mobile charges are generated in the tips, even at low densities (10^{16} cm^{-3}), these charges can diffuse under

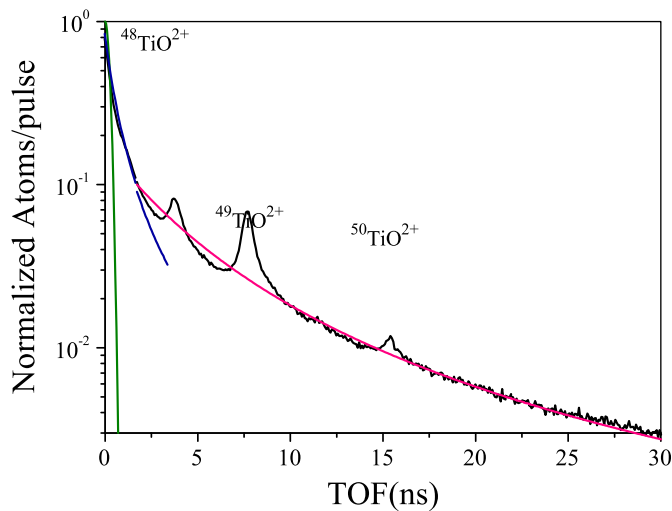


Fig. 22. Flight time spectrum of TiO^{2+} peaks for UV light (black line) à 20% of FR. Blue and pink lines correspond to the fit using Eq. (5). Fits values for blue line: $Q_n=0.17$ eV; $T_{\text{rise}}=250$ K and $\tau=1$ ns; for pink line: $Q_n=0.17$ eV; $T_{\text{rise}}=250$ K and $\tau=4$ ns. The detector timing accuracy is indicated in green. (For interpretation of the references to color in this figure caption, the reader is referred to the web version of this article.)

the effect of static field and contribute to the screening. In addition these free charges at the surface can absorb the laser energy directly on the surface. So, how can we differentiate between absorption due to surface defects and that due to free surface charges under high field?

More information on the evaporation time and on the temperature rise at the tip surface is necessary to answer this question.

5.3. Conclusions

Recent studies on oxides in LA-APT show that coating dielectric sample with a metallic layer is not even necessary for a few microns of bulk oxide on a metallic pre-tip. Indeed, the dielectric is already highly polarized due to the high field and, under laser illumination, with the generation of free charges, the field is well screened at the surface.

In addition, if only the metal layer absorbs the light no charges are created in the dielectric and the static electric field will penetrate inside the oxide. Thus, even if, through the absorption of the metal layer, the tip temperature becomes high enough to allow the evaporation, it will not be well controlled.

Finally, the metal layer should also ensure a rapid cooling of the tip apex. However, in the case of surface absorption under high electric field, the cooling time is fast, in any case.

In conclusion, the metallic coating of large band gap oxides is not the best solution for the analysis of these materials in LA-APT. It would be better to determine the factors that cause the confinement of the absorption at the apex of oxide tips and their dependence on the laser parameters to optimize evaporation.

To obtain this, new information is necessary on surface absorption under high electric field. New experimental configurations must be set-up.

6. General conclusions and perspectives

In order to understand the laser-assisted evaporation phenomena involved in LA-APT, it is necessary to study the mechanisms of interaction of ultra short laser pulses with a sub-wavelength tip. Due to the particular tip shaped geometry and to its small size

(radius of curvature of the tip of the order of a few tens of nanometer), several factors such as light diffraction effects at the discontinuity tip/vacuum; field enhancement at the tip apex, nonlinear optical effects during the interaction with the laser light, and surface plasmon resonance of the 'nano particle' represented by the apex have to be taken into account. All these effects have been discussed and their contribution to the evaporation behavior of metallic sample is now identified.

Indeed, LA-APT has been used as an original and very efficient tool for the analysis of the optical properties of metallic nano-objects. The results of this study are helpful to understand the evaporation mechanisms of metal tips under laser illumination, the inhomogeneous ablation mechanism of metallic nanoparticles when a fs laser is used [81] and the mechanism of the expansion under laser illumination of nanometric tips used for near field imaging [16].

Concerning nonmetallic samples, it is possible to obtain good analysis of these materials in LA-APT, but the reasons for this success are not yet clear. Indeed, at the low temperatures used in LA-APT (about 50 K) all free charges due to defects or doping are 'frozen'. Under these circumstances, then the static electric field cannot be screened and penetrates inside the sample. If the field penetrates inside the sample, the evaporation should happen in larger molecular clusters. Again, the LA-APT has been used as a unique tool for the study of laser-semiconductor interaction under a strong electric field, to investigate and understand how the laser can allow the controlled evaporation of the tip.

In addition, during the first analysis of large band gap oxides in LA-APT, the role of defects was highlighted. How are these defects formed? Are they from the sample preparation process by FIM milling? How does the laser-oxide interaction change when these defects are generated and when the sample is under a strong electric field? These questions are still unanswered and will be at the heart of future research.

Acknowledgments

The author would like to thank the many individuals at 'Groupe de Physique des Matériaux' from the l'University of Rouen who have contributed to this article, especially Bernard Deconihout, Francois Vurpillot, Jonathan Houard. Research was sponsored by the ANR Ultra-Sonde 2010 BLAN 0943 01 project and computer support from CINES of France under the project c20122085015.

References

- [1] D. Blavette, A. Bostel, J. Sarrau, B. Deconihout, A. Menand, *Nature* 363 (1993) 432.
- [2] D. Blavette, B. Deconihout, A. Bostel, J.M. Sarrau, M. Bouet, A. Menand, *The tomographic atom probe: a quantitative three-dimensional nanoanalytical instrument on an atomic scale*, *Review of Scientific Instruments* 64 (10) (1993) 2911–2919.
- [3] A. Cerezo, T. Godfrey, J. Hyde, S. Sijbrandij, G. Smith, *The tomographic atom probe: a quantitative three-dimensional nanoanalysis instrument on an atomic scale*, *Applied Surface Science* 76/77 (1994) 374–381.
- [4] M.K. Miller, A. Cerezo, M.G. Hetherington, G.D.W. Smith, *Atom Probe Field Ion Microscopy*, Oxford Science Publications - Clarendon Press, 1996.
- [5] D. Blavette, E. Cadel, A. Fraczkiewicz, A. Menand, *Science* 286 (1999) 5448.
- [6] M.N.T.T. Tsong, J.H. Block, B. Viswanatha, *Photon stimulated field ionization*, *Journal of Chemical Physics* 65 (6) (1976) 2469.
- [7] B. Viswanathan, W. Drachsel, J. Block, T. Tsong, *Journal of Chemical Physics* 70 (1979) 2582.
- [8] S. Nishigaki, W. Drachsel, J. Block, *Photon-induced field ionization mass spectrometry of ethylene on silver*, *Surface Science* 87 (2) (1979) 389–409.
- [9] T.T. Tsong, *Pulsed-laser-stimulated field emission from metal and semiconductor surfaces*, *Physical Review B* 30 (9) (1984) 4946.
- [10] A. Cerezo, C.R.M. Grovenor, G.D.W. Smith, *Pulsed laser atom probe analysis of semiconductor materials*, *Journal of Microscopy* 142 (1986) 155.
- [11] T.F. Kelly, M.K. Miller, *Invited review article: atom probe tomography*, *Review of Scientific Instruments* 78 (2007) 31101.

- [12] V.A. Ukraintsev, J.T. Yates Jr., *Journal of Applied Physics* 80 (1996) 2561.
- [13] P. Hommelhoff, Y. Sortais, A. Aghajani-Talesh, M. Kasevich, Field emission tip as a nanometer source of free electron femtosecond pulses, *Physical Review Letters* 96 (7) (2006) 77401.
- [14] C. Ropers, D. Solli, C. Schulz, C. Lienau, T. Elsaesser, Localized multiphoton emission of femtosecond electron pulses from metal nanotips, *Physical Review Letters* 98 (4) (2007) 43907.
- [15] A. Bouhelier, M. Beversluis, A. Hartschuh, L. Novotny, Near-field second-harmonic generation induced by local field enhancement, *Physical Review Letters* 90 (1) (2003) 13903.
- [16] A. Chimmalgı, C.P. Grigoropoulos, K. Komvopoulos, *Journal of Applied Physics* 97 (10) (2005) 104319.
- [17] A. Vella, B. Deconihout, L. Marrucci, E. Santamato, *Physical Review Letters* 99 (4) (2007) 46103.
- [18] J. Houard, A. Vella, F. Vurpillot, B. Deconihout, *Physical Review B* 81 (12) (2010) 125411.
- [19] T. Tsong, Field penetration and band bending near semiconductor surfaces in high electric fields, *Surface Science* 81 (1) (1979) 28–42.
- [20] L. Ernst, On the field penetration into semiconductors in the field ion microscope, *Surface Science* 85 (2) (1979) 302–308.
- [21] E. Mueller, *Physical Review* 103 (1956) 618.
- [22] R. Gomer, *Journal of Chemical Physics* 31 (1951) 341.
- [23] T.T. Tsong, *Journal of Physics F: Metal Physics* 8 (1978) 1349.
- [24] G.G. Rusina, S. Ereneevev, S.B. Borisdava, F. Sklyadnea, E. Chulkov, Surface phonon on al(111) surface, *Physical Review B* 71 (2005) 245401.
- [25] G. Kellogg, *Physical Review B* 29 (8) (1984) 4304.
- [26] G. Kellogg, T. Tsong, *Journal of Applied Physics* 51 (1980) 1184.
- [27] G. Kellogg, Determining the field emitter temperature during laser irradiation in the pulsed laser atom probe, *Journal of Applied Physics* 52 (1981) 5320.
- [28] M. Lee, R. Refenberger, E. Robins, H. Lindenmayr, Thermally enhanced field emission, *Journal of Applied Physics* 51 (1980) 4996.
- [29] H. Liu, H. Liu, T. Tsong, Numerical calculation of the temperature distribution and evolution of the field-ion emitter under pulsed and continuous-wave laser irradiation, *Journal of Applied Physics* 59 (4) (1986) 1334.
- [30] H. Liu, T. Tsong, Numerical calculation of the temperature evolution and profile of the field-ion emitter in the pulsed-laser time of flight atom probe, *Review of Scientific Instruments* 55 (11) (1984) 1779.
- [31] M. Lee, E. Robins, Thermal relaxation, *Journal of Applied Physics* 65 (1989) 1699.
- [32] T. Tsong, *Atom-Probe Field Ion Microscopy: Field Ion Emission and Surfaces and Interfaces at Atomic Resolution*, Cambridge University Press, 1990.
- [33] F. Vurpillot, B. Gault, A. Vella, M. Bouet, B. Deconihout, Estimation of the cooling times for a metallic tip under laser illumination, *Applied Physics Letters* 88 (2006) 094105.
- [34] B. Gault, F. Vurpillot, A. Bostel, A. Menand, B. Deconihout, *Applied Physics Letters* 86 (2005) 094101.
- [35] Y.R. Shen, *The Principles of Nonlinear Optic*, Wiley-Interscience Publication, 1984.
- [36] K. Kawase, J. Ichi Shikata, H. Ito, Terahertz wave parametric source, *Journal of Physics D: Applied Physics* 34 (2001) R1–R4.
- [37] A.V. Bragas, S.M. Landi, O.E. Martinez, Laser field enhancement at the scanning tunneling microscope junction measured by optical rectification, *Applied Physics Letters* 72 (1998) 2075–2077.
- [38] J.E. Sipe, V.C.Y. So, M. Fukui, G.I. Stegeman, Analysis of second-harmonic generation at metal surfaces, *Physical Review B* 21 (1980) 4389–4402.
- [39] M. Bass, P. Franken, J. Ward, G. Weinreich, Optical rectification, *Physical Review Letters* 9 (11) (1962) 446.
- [40] J. Rudnick, E.A. Stern, Second-harmonic radiation from metal surfaces, *Physical Review B* 4 (12) (1971) 4274–4290.
- [41] L. Novotny, R.X. Bian, X.S. Xie, Theory of nanometric optical tweezers, *Physical Review Letters* 79 (4) (1997) 645.
- [42] A. Vella, M. Gilbert, A. Hideur, F. Vurpillot, B. Deconihout, Ultra-fast ion emission from a metallic tip excited by femtosecond laser pulses, *Applied Physics Letters* 89 (2006) 251903.
- [43] A. Cerezo, P. Clifton, A. Gombert, G. Smith, Aspects of the performance of a femtosecond laser-pulsed 3-dimensional atom probe, *Ultramicroscopy* 107 (9) (2007) 720–725.
- [44] A. Cerezo, G. Smith, P. Clifton, Measurement of temperature rises in the femtosecond laser pulsed three-dimensional atom probe, *Applied Physics Letters* 88 (2006) 154103.
- [45] G. Sha, A. Cerezo, G. Smith, Field evaporation behavior during irradiation with picosecond laser pulses, *Applied Physics Letters* 92 (2008) 043503.
- [46] A. Etienne, Thèse de doctorat, Université de Rouen (November 2010).
- [47] F. Vurpillot, J. Houard, A. Vella, B. Deconihout, *Journal of Physics D: Applied Physics* 42 (12) (2009) 125502.
- [48] A. Vella, J. Houard, F. Vurpillot, B. Deconihout, Ultrafast emission of ions during laser ablation of metal for 3d atom probe, *Applied Surface Science* 255 (10) (2009) 5154–5158.
- [49] E. Palik, G. Ghosh, *Handbook of Optical Constants of Solids*, Academic Press, 1985.
- [50] J. Hohlfeld, S.S. Wellershoff, J. Gudde, U. Conrad, V. Jahnke, E. Matthias, *Chemical Physics* 251 (1–3) (2000) 237–258.
- [51] J. Chen, J. Beraun, Numerical study of ultrashort laser pulse interactions with metal films, *Numerical Heat Transfer Part A: Applications* 40 (1) (2001) 1–20.
- [52] B. Gault, A. Vella, F. Vurpillot, A. Menand, D. Blavette, B. Deconihout, Optical and thermal processes involved in ultrafast laser pulse interaction with a field emitter, *Ultramicroscopy* 107 (9) (2007) 713–719.
- [53] J. Houard, A. Vella, F. Vurpillot, B. Deconihout, Three-dimensional thermal response of a metal subwavelength tip under femtosecond laser illumination, *Physical Review B* 84 (3) (2011) 033405.
- [54] M. Gilbert, F. Vurpillot, A. Vella, H. Bernas, B. Deconihout, Some aspects of the silicon behaviour under femtosecond pulsed laser field evaporation, *Ultramicroscopy* 107 (9) (2007) 767–772.
- [55] B. Mazumder, A. Vella, M. Gilbert, B. Deconihout, G. Schmitz, Reneutralization time of surface silicon ions on a field emitter, *New Journal of Physics* 12 (2010) 113029.
- [56] G. Kellogg, T. Tsong, Pulsed-laser atom-probe field-ion microscopy, *Journal of Applied Physics* 51 (2) (1980) 1184–1193.
- [57] S. Koelling, N. Innocenti, A. Schulze, M. Gilbert, A. Kambham, W. Vandervorst, In-situ observation of non-hemispherical tip shape formation during laser-assisted atom probe tomography, *Journal of Applied Physics* 109 (2011) 104909.
- [58] D. Miller, D. Chemla, S. Schmitt-Rink, Relation between electroabsorption in bulk semiconductors and in quantum wells: the quantum-confined Franz-Keldysh effect, *Physical Review B* 33 (10) (1986) 6976.
- [59] E. Silaeva, N. Shcheblanov, T. Itina, A. Vella, J. Houard, N. Sévelin-Radiguet, F. Vurpillot, B. Deconihout, Numerical study of femtosecond laser-assisted atom probe tomography, *Applied Physics A: Materials Science & Processing* (2011) 1–5.
- [60] B. Mazumder, A. Vella, F. Vurpillot, G. Martel, B. Deconihout, Surface carrier recombination of a silicon tip under high electric field, *Applied Physics Letters* 97 (2010) 073104.
- [61] G. Kellogg, Field ion microscopy and pulsed laser atom-probe mass spectroscopy of insulating glasses, *Journal of Applied Physics* 53 (9) (1982) 6383–6386.
- [62] R. Stoian, A. Rosenfeld, D. Ashkenasi, I.V. Hertel, N.M. Bulgakova, E.E. B. Campbell, Surface charging and impulsive ejection during ultrashort pulsed laser ablation, *Physical Review Letters* 88 (2002) 097603.
- [63] M. Kuduz, G. Schmitz, R. Kirchheim, Investigation of oxide tunnel barriers by atom probe tomography (tap), *Ultramicroscopy* 101 (2) (2004) 197–205.
- [64] D. Blavette, F. Vurpillot, B. Deconihout, A. Menand, Atom probe tomography: 3d imaging at the atomic level, *Fabrication and Characterization in the Micro Nano Range* (2011) 201–222.
- [65] B. Mazumder, A. Vella, B. Deconihout, et al., Evaporation mechanisms of MgO in laser assisted atom probe tomography, *Ultramicroscopy* 111 (6) (2011) 571–575.
- [66] Y. Chen, T. Ohkubo, M. Kodzuka, K. Morita, K. Hono, Laser-assisted atom probe analysis of zirconia/spinel nanocomposite ceramics, *Scripta Materialia* 61 (7) (2009) 693–696.
- [67] K. Hono, T. Ohkubo, Y. Chen, M. Kodzuka, K. Oh-Ishi, H. Sepehri-Amin, F. Li, T. Kinno, S. Tomiya, Y. Kanitani, Broadening the applications of the atom probe technique by ultraviolet femtosecond laser, *Ultramicroscopy* 111 (6) (2011) 576–583, <http://dx.doi.org/10.1016/j.ultramic.2010.11.020>.
- [68] F. Li, T. Ohkubo, Y. Chen, M. Kodzuka, F. Ye, D. Ou, T. Mori, K. Hono, Laser-assisted three dimensional atom probe analysis of dopant distribution in Gd-doped CeO₂, *ScriptaMaterialia*, <http://dx.doi.org/10.1016/j.scriptamat.2010.04.029>.
- [69] E. Talbot, R. Lardé, F. Gourbilleau, C. Dufour, P. Pareige, Si nanoparticles in SiO₂ an atomic scale observation for optimization of optical devices, *EPL (Europhysics Letters)* 87 (2009) 26004.
- [70] E. Marquis, N. Yahya, D. Larson, M. Miller, R. Todd, Probing the improbable: imaging C atoms in alumina, *Materials Today* 13 (10) (2010) 34–36.
- [71] Y. Chen, T. Ohkubo, K. Hono, Laser assisted field evaporation of oxides in atom probe analysis, *Ultramicroscopy* 111 (6) (2011) 562–566.
- [72] M. Tsukada, H. Tamura, K. McKenna, A. Shluger, Y. Chen, T. Ohkubo, K. Hono, Mechanism of laser assisted field evaporation from insulating oxides, *Ultramicroscopy* 111 (6) (2011) 567–570.
- [73] A. Gibson, R. Haydock, J. LaFemina, Stability of vacancy defects in MgO: the role of charge neutrality, *Physical Review B* 50 (4) (1994) 2582–2592.
- [74] A. Gibson, R. Haydock, J. LaFemina, The electronic structure of neutral and charged surface vacancy defects in periclase, *Applied Surface Science* 72 (4) (1993) 285–293.
- [75] N. Daude, C. Gout, C. Jouanin, Electronic band structure of titanium dioxide, *Physical Review B* 15 (6) (1977) 3229–3235.
- [76] M. Ramamoorthy, R. King-Smith, D. Vanderbilt, Defects on TiO₂(110) surfaces, *Physical Review B* 49 (11) (1994) 7709–7715.
- [77] A. Plech, V. Kotaidis, M. Lorenc, J. Boneberg, Femtosecond laser near-field ablation from gold nanoparticles, *Nature Physics* 2 (2006) 44–47.